

Structure-Guided Development of Small-Molecule PRC2 Inhibitors Targeting EZH2–EED Interaction

Daohai Du,¹ Dandan Xu,¹ Licheng Zhu,¹ Giulia Stazi, Clemens Zwergel, Yanli Liu, Zhongyuan Luo, Yuanqing Li, Yuanyuan Zhang, Kongkai Zhu, Yiluan Ding, Jingqiu Liu, Shijie Fan, Kaiyan Zhao, Naixia Zhang, Xiangqian Kong, Hualiang Jiang, Kaixian Chen, Kehao Zhao, Sergio Valente,* Jinrong Min,* Wenhui Duan,* and Cheng Luo*



Cite This: *J. Med. Chem.* 2021, 64, 8194–8207



Read Online

ACCESS |



Metrics & More

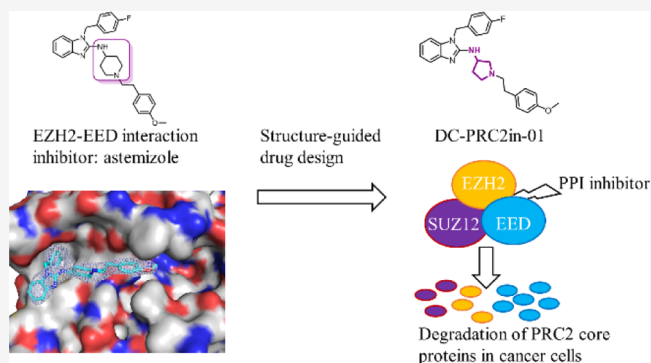


Article Recommendations



Supporting Information

ABSTRACT: Disruption of EZH2–embryonic ectoderm development (EED) protein–protein interaction (PPI) is a new promising cancer therapeutic strategy. We have previously reported the discovery of astemizole, a small-molecule inhibitor targeting the EZH2–EED PPI. Herein, we report the cocrystal structure of EED in complex with astemizole at 2.15 Å. The structure elucidates the detailed binding mode of astemizole to EED and provides a structure-guided design for the discovery of a novel EZH2–EED interaction inhibitor, DC-PRC2in-01, with an affinity K_d of 4.56 μ M. DC-PRC2in-01 destabilizes the PRC2 complex, thereby leading to the degradation of PRC2 core proteins and the decrease of global H3K27me3 levels in cancer cells. The proliferation of PRC2-driven lymphomas cells is effectively inhibited, and the cell cycle is arrested in the G0/G1 phase. Together, these data demonstrate that DC-PRC2in-01 could be an effective chemical probe for investigating the PRC2-related physiology and pathology and providing a promising chemical scaffold for further development.



INTRODUCTION

In mammals, polycomb group (PcG) proteins, which mainly assemble into two major kinds of enzymatic complexes, polycomb repressive complex 1 (PRC1) and PRC2,¹ are a family of proteins responsible for chromatin compaction and transcriptional repression during early development and throughout adulthood.^{2–6} PRC2 exhibits a methyltransferase activity to generate mono-, di-, or trimethylation for histone H3 at lysine 27 (H3K27me1/me2/me3), which requires the assembly integration and mutual interactions of three core proteins: the enhancer of zeste homologue 1/2 (EZH1/2), embryonic ectoderm development (EED) protein, and the suppressor of zeste 12 homologue (SUZ12).^{7–9} The PRC2 complex also comprises other accessory proteins, such as RbAp46/48, JARID2, and AEBP2.⁴ The gene silencing H3K27me3 mark is implicated in the recruitment of repressive regulators, such as PRC1, catalyzing the monoubiquitination of histone H2A at lysine-119 (H2AK119ub1).^{10,11} In addition, H3K27me3 could be recognized by the EED aromatic cage and subsequently allosterically stimulate the activity of PRC2 via inducing a helix formation of the stimulation-responsive motif in EZH2.^{12–14}

Previous studies have reported that abnormal activity of PRC2 and hypermethylation of H3K27 were observed in

multiple human malignancies.^{15–17} EZH2 is overexpressed in several solid tumors^{18–23} and heterozygous gain-of-function mutations within the SET domain of EZH2 highly occur in germinal center B-cell type diffuse large B-cell lymphoma (GCB-DLBCL) and follicular lymphoma (FL).^{24–26} Due to the oncogenic properties of EZH2,²⁷ selective small-molecule S-adenosylmethionine (SAM)-competitive EZH2 inhibitors have been extensively developed,^{28–33} such as GSK126,³⁴ CPI-1205,³⁵ and tazemetostat (EPZ-6438),^{36,37} which have advanced into the clinical trial phases. Recently, tazemetostat has been approved by Food and Drug Administration (FDA) for the treatment of advanced epithelioid sarcoma and FL.^{38,39} In addition to EZH2 as a cancer therapeutic target, targeting the H3K27me3 binding pocket of EED is a promising alternative strategy to suppress the PRC2 activity in cancers,⁴⁰ especially when we need to deal with acquired resistance to

Received: December 30, 2020

Published: June 2, 2021



EZH2 inhibitors.^{38,41} The representative EED inhibitors EED226,^{42,43} A-395,⁴⁴ BR-001,⁴⁵ and EEDi-5285⁴⁶ displayed strong selective and potential antilymphoma activity in preclinical xenograft models, likewise in EZH2 inhibitor-resistant models. Thus far, only MAK683, a derivative of EED226, has entered the phase 1/2 clinical trials.^{17,38,46}

Besides the catalytic site of EZH2 and H3K27me3 binding pocket of EED, another promising strategy against PRC2 activity is disrupting the interaction between EZH2 and EED.^{38,47,48} Previous structural and biochemical studies have revealed that the α -helix EED-binding domain (EBD) of EZH2 binds to the bottom of the WD40 repeat domain of EED,⁴⁹ opposite to the EED aromatic cage, and a stabilizing α -helix of EZH2 (SAH-EZH2) peptide selectively disrupts the EZH2–EED complex and inhibits the PRC2 activity *in vitro*,⁵⁰ indicating the druggability of protein–protein interaction (PPI) between EZH2 and EED. Furthermore, the first reported EZH2–EED PPI inhibitor astemizole has demonstrated that small-molecule compounds could bind to the large interface of the EZH2–EED PPI and destabilize the PRC2 complex, thereby leading to H3K27me3 decrease and cell proliferation arrest in PRC2-dependent DLBCL.⁵¹ Astemizole is an antiallergy drug repurposing as a novel EZH2–EED interaction inhibitor, highlighting the good effects of drug repurposing, which is also evidenced by antimalaric agent hydroxychloroquine, as a novel EED inhibitor.⁵² To the best of our knowledge, there is no report about the structure of EED in complex with small-molecular inhibitors targeting the EZH2–EED interaction. Herein, we disclose the binding mode of astemizole to EED using the X-ray crystal structure, and report the structure-guided discovery of novel inhibitors targeting the EZH2–EED interaction as a promising therapeutic strategy for PRC2-dependent lymphomas. Our results show that DC-PRC2in-01 disrupts the EZH2–EED interaction with a single-digit micromolar activity under *in vitro* conditions.

RESULTS AND DISCUSSION

Determination of the Crystal Structure of EED in Complex with Astemizole and Molecular Design. To elucidate the detailed binding mode of astemizole by EED and to facilitate the EZH2–EED inhibitor design, we have determined the crystal structure of astemizole in complex with EED (aa 40–441) (PDB ID: 7KXT, Table 1). As shown in Figure 1, EED folds into a typical seven-bladed β -propeller structure, with astemizole binding to the bottom of the WD40-repeat domain, where EED recognizes the EZH2 peptide (aa 39–68) (Figure 1F,G).⁴⁹ The binding site accommodating astemizole is composed of 13 residues (L246, L315, L318, C330, M336, L353, F372, W373, Q374, L391, V393, P396, and H397) (Figure 1B,E). Astemizole binds to this site with the fluorobenzene group inserting deeply into a hydrophobic pocket formed by six residues (L315, C330, L391, V393, P396, and H397). Compared with the structure of the EZH2 peptide bound to EED, this fluorobenzene group occupies the space of the hot-spot residue F42 of EZH2 (Figure 1F,G). The benzimidazole moiety establishes interactions with hydrophobic residues L318, M336, and L353. In addition to the fluorobenzene and benzimidazole groups, 4-methoxyphenethyl is also stabilized by hydrophobic interactions with L246, F372, W373, and Q374. Collectively, astemizole forms extensive hydrophobic interactions with EED with minimal polar interactions.

Table 1. X-ray Diffraction Data Collection and Refinement Statistics

		EED-astemizole
PDB code		7KXT
Data Collection		
space group		$P2_1$
cell dimensions		
a, b, c (Å)		81.47, 49.94, 105.32
α, β, γ (deg)		90, 105.11, 90
resolution (Å) (highest resolution shell)		40.39–2.15 (2.21–2.15)
measured reflections		148,840
unique reflections		44,346
R_{merge}		9.4 (71.3)
$I/\sigma I$		8.2 (1.4)
completeness (%)		98.7 (94.6)
redundancy		3.4 (3.1)
Refinement		
resolution (Å)		40.39–2.15
no. reflections (test set)		44,334 (2165)
$R_{\text{work}}/R_{\text{free}}$ (%)		17.8/21.5
no. atoms		
protein		5799
ligand		68
water		98
B-factors (Å ²)		
protein		41.0
ligand		52.2
water		35.9
rmsd		
bond lengths (Å)		0.008
bond angles (°)		0.9
ramachandran plot % residues		
favored		95.96
additional allowed		4.04
generously allowed		0.0
disallowed		0.0

Astemizole binds to the EZH2–EED interaction interface, which is different from the binding modes of EZH2 inhibitors and EED inhibitors (Supporting Information Figure S2). EZH2 inhibitors bind to the SAM binding pocket in the SET domain of EZH2, and EED inhibitors bind to the H3K27me3 binding pocket at the top of WD40 repeat domain of EED. Both binding sites are narrow and deep suitable for the accommodation of small molecules, while the large and wide interface between EZH2 and EED (more than 3000 Å² of the buried surface area)⁵¹ is an inevitable question about the chemical tractability in the past.⁵³ The crystal structure of astemizole in complex with EED directly demonstrates that the EZH2–EED interaction interface could be targeted by small molecules.

Because the complex structure shows that astemizole engages the large groove of the PPI interface of EZH2–EED via hydrophobic contacts, the following strategies of astemizole optimization were proposed as depicted in Figure 2. We first hypothesized that the inhibitory potency would be remarkably improved if a hydrogen bond was formed by installing a hydrogen bond acceptor (HBA) or a hydrogen bond donor (HBD). Meanwhile, further exploration of hydrophobic interactions is also necessary as most of the surrounding residues are hydrophobic. Besides, 4-aminopiperidine of astemizole is adjacent to the backbones of L315, Q374, and

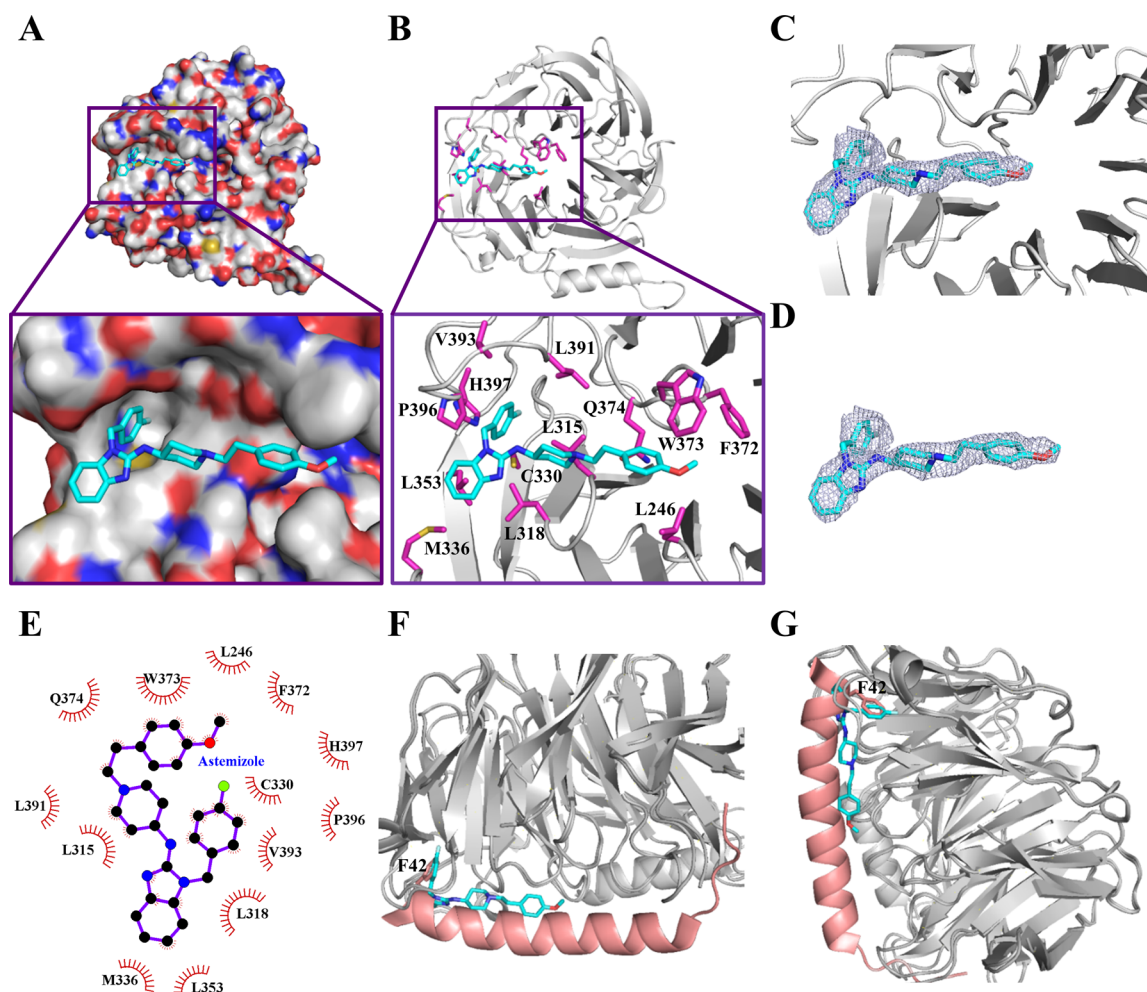


Figure 1. Structural analysis of EED in complex with astemizole. (A,B) Overview and close-up view of EED (surface and cartoon representations, respectively) in complex with astemizole (sticks in cyan). The surrounding residues in EED are shown as sticks in magenta. (C,D) Cartoon representation of EED with the Fo-Fc omit electron density map for compound astemizole contoured at 2.5σ levels. (E) Schematic diagram showed the hydrophobic interactions (shown as starbursts) of astemizole with EED. (F,G) Superposition of astemizole (cyan sticks) and the EZH2 peptide (salmon cartoon) in complex with EED (gray cartoon) (PDB ID: 2QXV and 7KXT).

L391, implying that additional hydrogen bonds might be introduced at this moiety. Along with the pivotal role in molecular configuration, the stereochemical structure 4-aminopiperidine may provide another potential for optimization.

Structure–Activity Relationship (SAR) Exploration.

With the goal of introducing additional hydrogen bonds to improve biochemical potency, HBAs or HBDs were employed at different parts of astemizole such as NO_2 , NH_2 , OH , F , and CF_3 , intending to present within the hydrogen bond distance with the backbone carbonyl or amino of surrounding residues. During the initial course of optimization, 4-aminopiperidine was kept unchanged. As shown in Table 2, modifications of benzyl at the *p*-, *m*-, or *o*-position (1–2, 4–6) retained comparable activities to astemizole, revealing that the benzyl moiety could accommodate diverse electron-withdrawing groups (EWGs). The addition of an amino group to either position of benzimidazole (7–10) also made no significant differences, which might be due to the fact that benzimidazole occupies the margin of EED and it is particularly difficult to form stable interactions here. Subsequently, introduction of the *m*-hydroxyl group at the terminal phenyl (12) maintained the

potency, while others (11, 13–14) caused an obvious loss in inhibitory activities.

Then, our efforts switched to explore the hydrophobic interactions as illustrated in Figure 2. Perhaps, EWGs at benzyl (1–2, 4–6) contributed to more stable van der Waals on account of the electronic effect. Therefore, the increased hydrophobicity of compounds at benzyl (15–16, in Table 3) was found to be detrimental to biochemical potency. However, the terminal hydrophobic groups, methoxy (astemizole) and methyl (18), were preferred to maintain the potency compared with the hydrogen atom (17) possibly owing to more hydrophobic contacts, which was consistent with the results obtained from compounds 11, 13, and 14.

We next turned our attention to 4-aminopiperidine with an attempt to exploit the optimal distance of the two nitrogen atoms to introduce additional hydrogen bonds. As shown in Table 4, structurally diverse saturated and aromatic rings as well as chains were chosen for the replacement of 4-aminopiperidine, with the emphasis on structures containing at least two nitrogen atoms acting as an expected dual HBA or HBD. First, the nitrogen atom was moved from piperidine to Linker2 to afford compounds 19 and 20. Compound 19 demonstrated a significant loss in potency as a result of its *cis*-

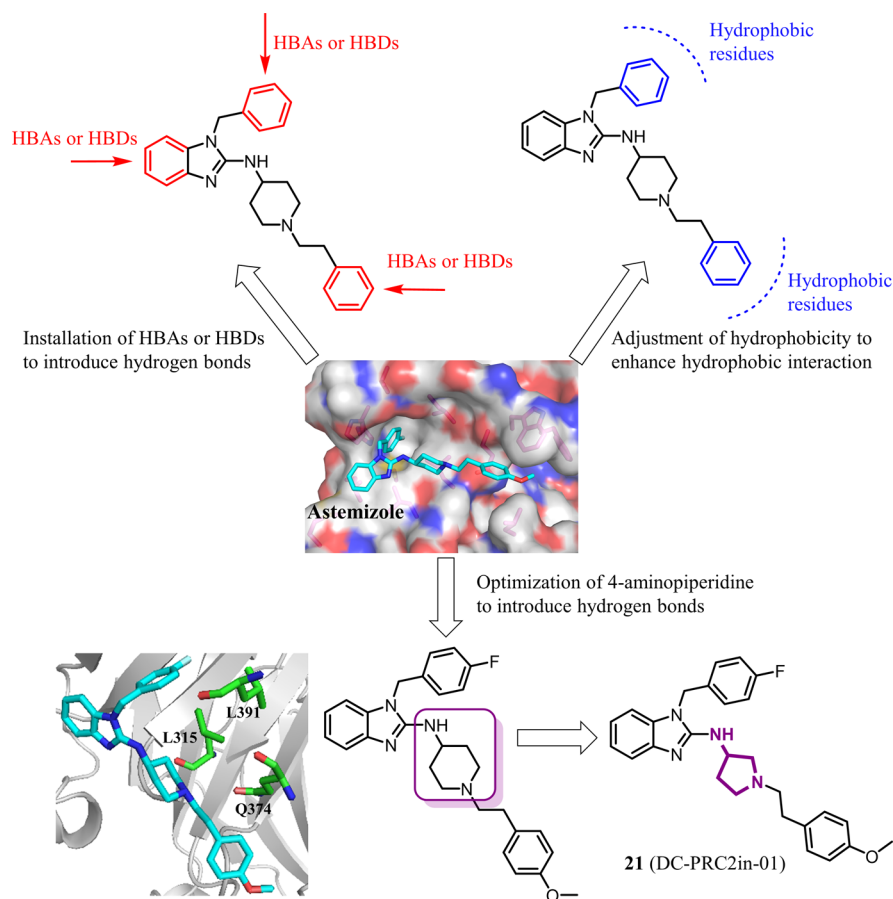


Figure 2. Structure-guided design and optimization of new EZH2–EED interaction inhibitors.

configuration. Then, 4-aminopiperidine was changed into 3-aminopyrrolidine to make the two nitrogen atoms closer as well as to adjust the molecular configuration. Gratifyingly, compounds (**21–23**) containing 3-aminopyrrolidine exhibited a more than 15-fold improvement in potencies over astemizole and it made no difference between *S* (**22**) and *R* (**23**). It was probable that the hydrogen bonds were formed with adjacent residues L315, Q374, or L391 as expected. The distance of these two nitrogen atoms was further decreased to yield **24**, which displayed a 3-fold increase in activity compared with astemizole. Furthermore, we examined the impacts of rigidity and flexibility of molecules on biochemical activities. Aromatic compounds **25** and **26** were synthesized in order to enhance the molecular rigidity, both of which achieved slightly increased potencies. What is more, piperidine was opened to obtain two flexible chain structures **27** and **28**. Compound **27** also showed a significantly improved potency, while compound **28** on the opposite. In summary, the appropriate length between the two nitrogen atoms was critical to the formation of hydrogen bonds. 3-Aminopyrrolidine was considered as a more efficient spacer and compound **21** (DC-PRC2in-01) was selected for further investigation.

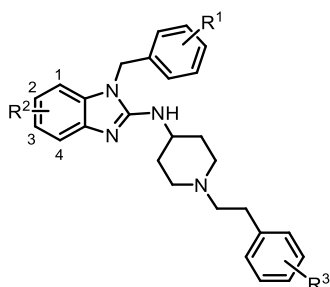
Determination of Binding Activity and Molecular Docking of DC-PRC2in-01 to EED. To characterize the binding activity of DC-PRC2in-01 (**21**) to the EED protein, we performed nuclear magnetic resonance (NMR) and surface plasmon resonance (SPR) assays, respectively. As expected, significant binding signals in both ligands' T1 ρ (Figure 3A) and saturation transfer difference (STD) spectra (Supporting Information Figure S3) were observed when DC-PRC2in-01

was incubated with the EED protein. Furthermore, at a concentration of more than 20 μ M, the EZH2 (aa 39–68) peptide almost completely recovered the T1 ρ signal of the compound, indicating that DC-PRC2in-01 directly binds to the interface between EZH2 and EED. The K_d value of DC-PRC2in-01 to the EED protein is 4.56 μ M measured by SPR (Figure 3B), which is equivalent to the IC₅₀ of 4.21 μ M determined by the fluorescence polarization (FP) competitive binding assay (Table 4 and Figure 3C). Taken together, these biophysical and biochemical results demonstrate that DC-PRC2in-01 reversibly and specifically binds to EED with a single-digit micromolar binding affinity.

To explore the molecular details of DC-PRC2in-01 in binding with EED, we performed molecular docking and found that three hydrogen bonds were formed between the two nitrogen atoms of DC-PRC2in-01 and carbonyl groups of residues W373, Q374, and L391 in EED (Figure 3D). This finding is consistent with our predictions as mentioned above. The benzimidazole moiety of DC-PRC2in-01 exposes to solvent without any contacts with the surrounding residues of EED (Supporting Information Figure S4), which indicates that this group might be further optimized in the future.

Disruption and Degradation of the PRC2 Core Complex and Decrease of H3K27me3 Levels in Pfeiffer Cells Induced by DC-PRC2in-01. Previous studies have suggested that the EZH2–EED interaction is critical for the stability and activity of the PRC2 complex.^{54–56} Accordingly, we evaluated the disruption activity of DC-PRC2in-01 to the PRC2 core complex in Pfeiffer cells, in which EZH2 harbors a A677G mutant and is more sensitive to the EZH2 inhibitors

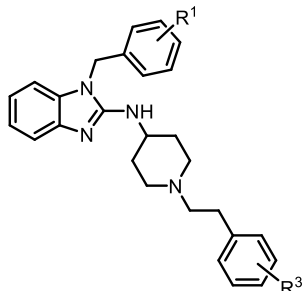
Table 2. Investigation of SAR by Introducing HBAs or HBDs



compd.	R ¹	R ²	R ³	FP assay (IC ₅₀ , μM) ^a
1	<i>p</i> -CF ₃		<i>p</i> -OCH ₃	60.8
2	<i>p</i> -NO ₂		<i>p</i> -OCH ₃	66.3
3	<i>p</i> -NH ₂		<i>p</i> -OCH ₃	221
4	<i>p</i> -F, <i>m</i> -F		<i>p</i> -OCH ₃	56.5
5	<i>p</i> -F, <i>m</i> -NO ₂		<i>p</i> -OCH ₃	61.6
6	<i>p</i> -F, <i>o</i> -NO ₂		<i>p</i> -OCH ₃	80.1
7	<i>p</i> -F	1-NH ₂	<i>p</i> -OCH ₃	73.8
8	<i>p</i> -F	2-NH ₂	<i>p</i> -OCH ₃	64.7
9	<i>p</i> -F	3-NH ₂	<i>p</i> -OCH ₃	63.6
10	<i>p</i> -F	4-NH ₂	<i>p</i> -OCH ₃	48.6
11	<i>p</i> -F		<i>p</i> -OH	190
12	<i>p</i> -F		<i>m</i> -OH	61.5
13	<i>p</i> -F		<i>o</i> -OH	175
14	<i>p</i> -F		<i>m</i> -NO ₂	341
astemizole	<i>p</i> -F		<i>p</i> -OCH ₃	74.2

^aIC₅₀ values reported as an average ≥2 determination.

Table 3. Investigation of SAR by Adjusting Hydrophobicity



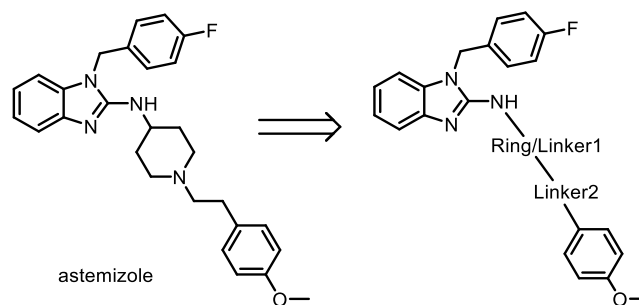
compd.	R ¹	R ³	FP assay (IC ₅₀ , μM) ^a
15	<i>p</i> -H	<i>p</i> -OCH ₃	131
16	<i>p</i> -CH ₃	<i>p</i> -OCH ₃	153
17	<i>p</i> -F	<i>p</i> -H	119
18	<i>p</i> -F	<i>p</i> -CH ₃	87.6
astemizole	<i>p</i> -F	<i>p</i> -OCH ₃	74.2

^aIC₅₀ values reported as an average ≥2 determination.

and EED inhibitors.^{34,42} As expected, after 72 h of exposure to different concentrations of DC-PRC2in-01, all of the PRC2 core proteins, EZH2, EED, and SUZ12, were dose-dependently depleted, especially for EED, which exhibited pronounced degradation at lower concentrations of DC-PRC2in-01 (Figure 4A). Our finding is in accordance with the previously reported effects of the EED lost-of-function mutations, the SAH-EZH2 peptides, and astemizole.^{50,51,55}

Currently, it is reported that EED could be directly degraded by proteolysis-targeting chimeras (PROTACs).^{57,58} The degradation of PRC2 core proteins induced by EED-directed PROTACs is an event-driven modality, while EZH2–

Table 4. Investigation of SAR by Replacing 4-Aminopiperidine



Compd.	Ring/Linker1	Linker2	FP assay (IC ₅₀ , μM) ^a
19			> 500
20			78.7
21			4.21
22			4.56
23			3.93
24			21.5
25			33.8
26			32.5
27			11.6
28			464
astemizole			74.2

^aIC₅₀ values reported as an average ≥2 determination.

EED PPI inhibitors belong to the traditional occupancy-driven paradigm. EED-directed PROTAC directly binds to the EED protein with its warhead specifically targeting the H3K27me3 binding pocket of EED protein, and recruits a specific E3 ubiquitin ligase with its ligand VHL (von Hippel-Lindau), resulting in EED protein ubiquitination and degradation via a ubiquitin protease system. While, for astemizole and its derivatives, they bind to EED protein on the interface between EZH2 and EED, and indirectly induce EED protein degradation via an unclear pathway, which deserves further research.

Because the H3K27me3 mark is primarily produced by the unique H3K27 methyltransferase PRC2, it is conceivable that the global H3K27me3 levels would decrease in the condition of depletion of the PRC2 core complex. Unsurprisingly, the treatment of Pfeiffer cells by DC-PRC2in-01 caused a dose-dependent loss of H3K27me3, which virtually disappeared at 10 μM (Figure 4A). The DC-PRC2in-01-mediated disruption of the EZH2 and EED interaction represents a novel mechanism of action (MOA) that inhibition of the PRC2 activity is attributed to disassembly of the PRC2 complex, distinct to the previously reported MOAs of SAM-competitive EZH2 inhibitors and EED-H3K27me3 inhibitors. By contrast, the other histone H3 trimethylation marks were not significantly affected, suggesting the specific inhibition of DC-PRC2in-01 to the PRC2 activity (Figure 4B). Overall, the above-mentioned results indicate that DC-PRC2in-01 specifically inhibits the PRC2 activity by disrupting the EZH2–EED

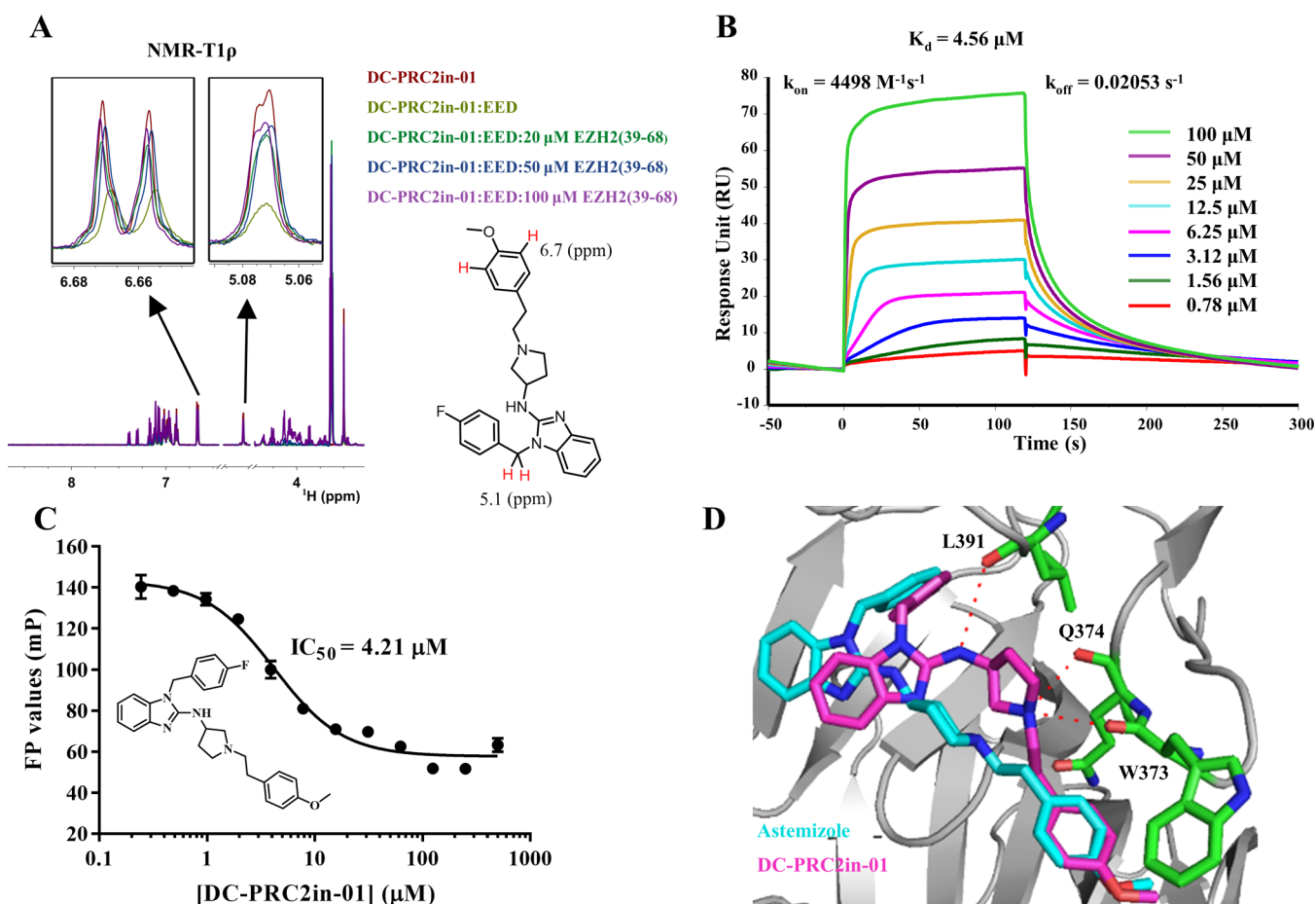


Figure 3. Characterization of binding activity of DC-PRC2in-01 to EED. (A) T1 ρ NMR spectra of DC-PRC2in-01 (red), DC-PRC2in-01 in the presence of EED (light green), and DC-PRC2in-01 in the presence of EED and 20 μ M (green) or 50 μ M (blue) or 100 μ M EZH2 peptide (purple). The four protons (red color) of DC-PRC2in-01 are shown correlated with the two insets. (B) Determination of binding affinity of DC-PRC2in-01 to EED by SPR. (C) FP competitive binding assay for IC₅₀ determination of DC-PRC2in-01. DC-PRC2in-01 dose-dependently displaced the FITC-labeled EZH2 peptide binding to EED. (D) Molecular docking model of DC-PRC2in-01 with EED. DC-PRC2in-01 (magenta sticks), not astemizole (cyan sticks), forms hydrogen bonds with residues W373, Q374, and L391 (green sticks) in EED (gray cartoon).

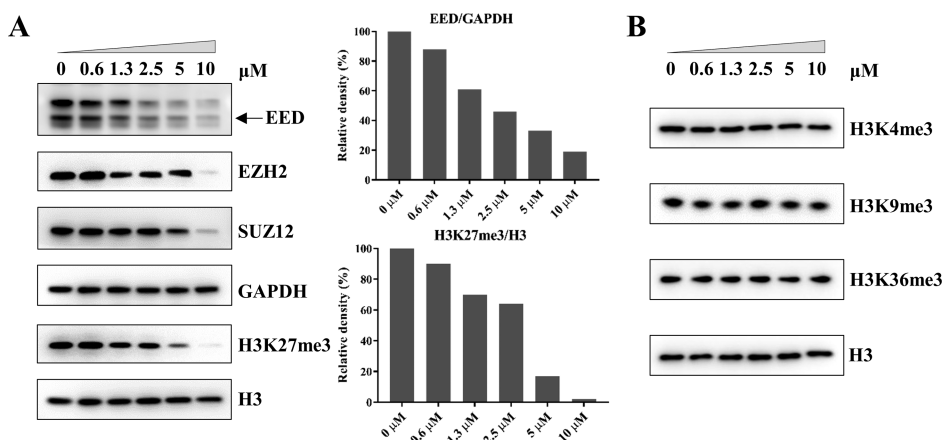


Figure 4. Effects of DC-PRC2in-01 on PRC2 core proteins, H3K27me3, and other histone H3 lysine trimethylation marks. (A) Western blotting analysis of EZH2, EED, SUZ12, and H3K27me3 in Pfeiffer cells treated with different concentrations of DC-PRC2in-01. Quantification of EED and H3K27me3 changes is represented in the bar graphs. Representative western blots of EED and H3K27me3 were normalized to corresponding GAPDH and total H3, respectively, and expressed as percent change in DC-PRC2in-01-treated versus DMSO-treated cells. (B) Western blots against other histone H3 lysine methylation marks in Pfeiffer cells treated with different concentrations of DC-PRC2in-01. Total histone H3 is used as a loading control.

interaction, leading to the depletion of core components of PRC2.

Antiproliferation Activity of DC-PRC2in-01 in PRC2-Dependent DLBCLs. Because previous studies reported that

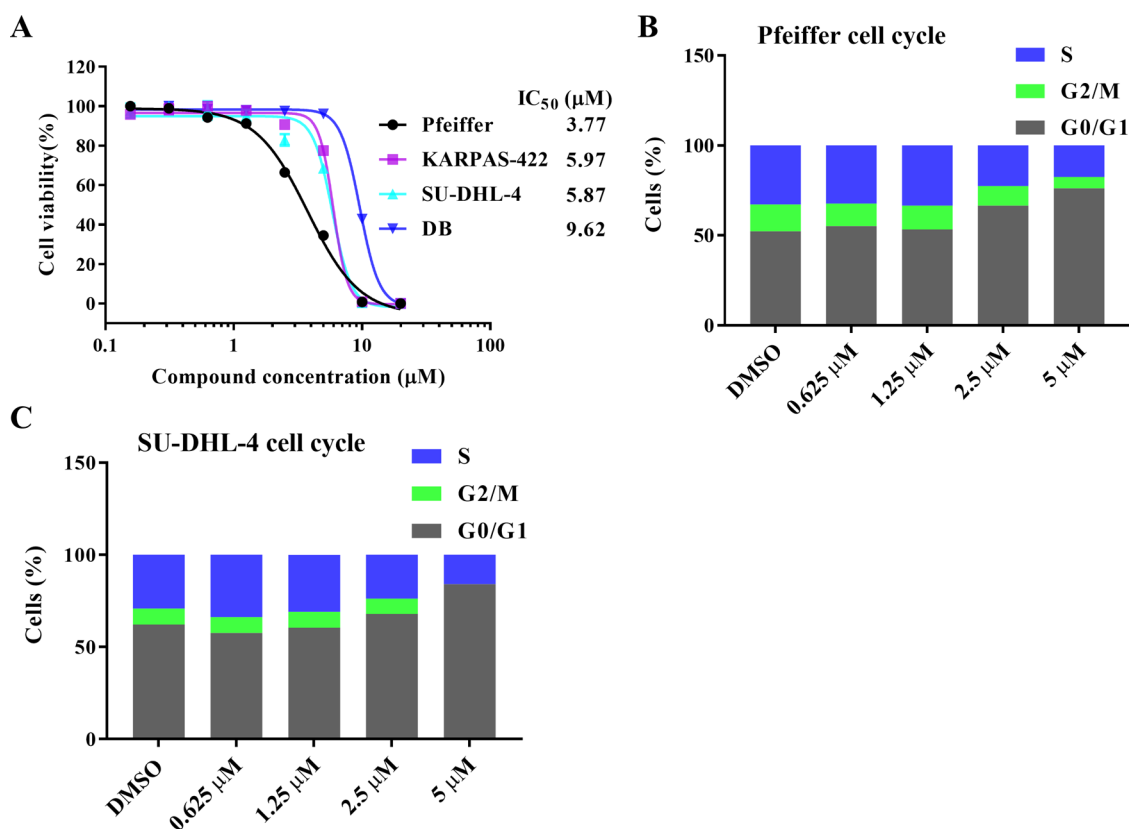


Figure 5. Growth inhibition effect of DC-PRC2in-01 on the DLBCL cells harboring gain-of-function mutation of EZH2. (A) Cell viability of four DLBCL cells treated with DC-PRC2in-01 for 3 days. (B,C) Cell cycle analysis in Pfeiffer cells and SU-DHL-4 cells during incubation with different concentrations of DC-PRC2in-01.

the growth of DLBCL cell lines carrying heterozygous mutation of EZH2 is dependent on the enhanced activity of PRC2,^{24,34} we measured the growth inhibition effects of DC-PRC2in-01 on these cancer cells, including Pfeiffer, KARPAS-422, SU-DHL-4, and DB, via a cell viability assay. As shown in Figure 5A, the proliferation of these cells was suppressed in a dose-dependent manner with all IC₅₀ below 10 μM. To note, Pfeiffer is the most sensitive cell line among DLBCLs, which is also observed with the treatment of the other PRC2 inhibitors targeting the catalytic domain of EZH2 or EED-H3K27me3 interaction.^{34,45}

To further explore the mechanism of proliferation arrest, we evaluated the impact of DC-PRC2in-01 on the cell cycle of DLBCL cells. As shown in Figure 5B,C, both Pfeiffer and SU-DHL-4 cells were dose-dependently arrested in the G0/G1 phase with a concurrent decrease of cells in G2/M and S. Compared to cells treated with DMSO controls, 5 μM of DC-PRC2in-01 led to an increase of cells in the G0/G1 phase from 52.3 to 76.2% and from 62.2 to 84% for Pfeiffer and SU-DHL-4 cells, respectively. Correspondingly, a decrease of Pfeiffer cells in G2/M and S phases from 14.9 to 6.2% and from 32.8 to 17.6%, and a decrease of SU-DHL-4 cells in G2/M and S phases from 8.6 to 0% and from 29.2 to 16%, were observed. These results suggest that the effect of DC-PRC2in-01 on DLBCL cell proliferation is owing to the reduction of cell fractions in G2/M and S phases.

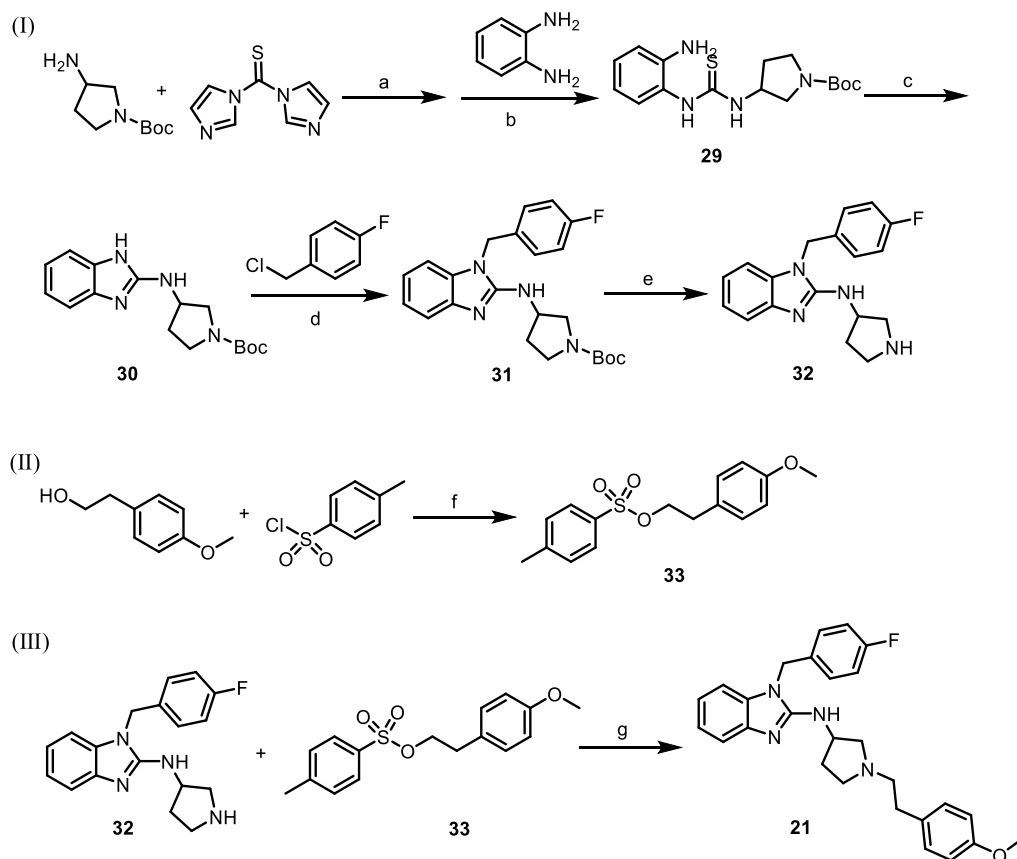
CHEMISTRY

A synthetic route to compound **21** is summarized in Scheme 1.^{59,60} Thiourea **29** was achieved through the acylation of *tert*-

butyl 3-aminopyrrolidine-1-carboxylate with thiocarbonyl diimidazole followed by the addition of *o*-phenylenediamine. Subsequent cyclization in the presence of iodomethane afforded the benzimidazole compound **30**. Alkylation of **30** with 4-fluorobenzyl chloride under alkaline conditions produced **31**. Then, deprotection of the Boc group using trifluoroacetic acid provided the key intermediate **32**, which reacted with arylethyl tosylate **33** to yield the target compound **21**. Synthetic routes to other compounds are described in the Supporting Information.

CONCLUSIONS

Starting from our previously discovered EZH2–EED interaction inhibitor astemizole, we disclosed the detailed binding mode of astemizole to EED by resolving their cocrystal structure and performed the structure-guided design and exploration to discover a novel inhibitor DC-PRC2in-01 with a more than 15-fold improvement in inhibitory activity over astemizole. The results of NMR- and SPR-based binding assays showed that DC-PRC2in-01 reversibly and specifically binds to EED with a binding affinity of $K_d = 4.56 \mu\text{M}$. DC-PRC2in-01 disrupted the EZH2–EED complex, and induced the degradation of the PRC2 core components and decrease of global H3K27me3 levels in cancer cells. The antiproliferation activity of DC-PRC2in-01 was determined in DLBCL cell lines with single-digit micromolar IC₅₀ values, and the MOA of growth inhibition is in part due to the cell cycle arrest in the G0/G1 phase. In summary, our work has advanced the development of a new potent inhibitor against, the EZH2–EED interaction. DC-PRC2in-01 could be an effective

Scheme 1. Synthesis of Compound 21^a

^aReagents and conditions: (a) CH₃CN, 0 °C to rt; (b) CH₃CN, 50 °C; (c) ICH₃, EtOH, reflux; (d) Na₂CO₃, DMF, 70 °C; (e) TFA, CH₂Cl₂, rt; (f) Et₃N, CH₂Cl₂, rt; and (g) Na₂CO₃, KI, DMF, 80 °C.

chemical probe for investigating the PRC2-related physiology and pathology and yet requires further development for targeted epigenetic therapy.

EXPERIMENTAL SECTION

General Information. All starting materials and reagents were purchased from commercial sources or prepared according to reference procedures. All purchased chemicals and solvents were used as received without further purification. All reactions were monitored by thin-layer chromatography on silica gel plates and visualized under UV light. Flash chromatography was performed using silica gel (300–400 mesh). ¹H NMR and ¹³C NMR spectra were generated in CDCl₃, CD₃OD, or DMSO-*d*₆ on Varian Mercury 300, 400, or 600 NMR spectrometers. Low-resolution mass spectra (ESI) were obtained using an Agilent 6110 Quadrupole LC/MS spectrometer. High-resolution mass (ESI) data were obtained using an Agilent G6520 Q-TOF LC-MS spectrometer. All tested compounds were purified using an Agilent Infinity 1260 high-performance liquid chromatograph coupled with a diode array detector and the ZORBAX Eclipse Plus column (C18, 4.6 × 150 mm, 5 μm). The eluent was 70 to 80% MeOH in 0.1% triethylamine aqueous solution with a flow rate of 1.0 mL/min. The analysis process lasted for 18 min and the purity was >95%.

Synthetic Procedures. *tert*-Butyl 3-((2-Aminophenyl)thioureido)pyrrolidine-1-carboxylate (**29**). To a solution of 1,1'-thiocarbonyldiimidazole (2.30 g, 12.9 mmol) in MeCN (30 mL) was added *tert*-butyl 3-aminopyrrolidine-1-carboxylate (2.00 g, 10.7 mmol) in MeCN (10 mL) dropwise at 0 °C. The mixture was then stirred at rt for 4 h. *O*-phenylenediamine (1.74 g, 16.1 mmol) was added and the resulting solution was stirred for an additional 3 h at 50 °C. The mixture was concentrated and purified by flash silica

chromatography (0 to 2% MeOH in CH₂Cl₂) to give **29** as a light-yellow solid (2.53 g, 70.0%), mp 173 °C. ¹H NMR (300 MHz, CDCl₃): δ 7.71 (s, 1H), 7.15 (t, *J* = 7.7 Hz, 1H), 7.02 (d, *J* = 7.8 Hz, 1H), 6.78 (d, *J* = 7.3 Hz, 1H), 6.75 (d, *J* = 7.6 Hz, 1H), 5.89 (s, 1H), 4.97–4.89 (m, 1H), 3.68 (dd, *J* = 11.6, 6.5 Hz, 1H), 3.40–3.25 (m, 2H), 3.19–3.08 (m, 1H), 2.25–2.17 (m, 1H), 1.90–1.75 (m, 1H), 1.42 (s, 9H). ESI-MS *m/z*: [M + H]⁺ 337.2.

tert-Butyl 3-((1H-Benzo[d]imidazole-2-yl)amino)pyrrolidine-1-carboxylate (**30**). A solution of **29** (2.50 g, 7.43 mmol) in EtOH (50 mL) was treated with iodomethane (1.39 mL, 22.3 mmol) in batches. The mixture was stirred at 70 °C for 2 h. The solution was concentrated and purified by flash silica chromatography (0 to 3% MeOH in CH₂Cl₂) to afford **30** as a light-yellow solid (1.41 g, 62.8%), mp 210–211 °C. ¹H NMR (300 MHz, CD₃OD): δ 7.32 (s, 2H), 7.09 (s, 2H), 4.32–4.24 (m, 1H), 3.78–3.56 (m, 2H), 3.56–3.37 (m, 2H), 2.37–2.25 (m, 1H), 2.11–2.00 (m, 1H), 1.47 (s, 9H). ESI-MS *m/z*: [M + H]⁺ 303.2.

tert-Butyl 3-((1-(4-Fluorobenzyl)-1H-benzo[d]imidazole-2-yl)amino)pyrrolidine-1-carboxylate (**31**). A mixture of **30** (1.39 g, 4.60 mmol), 1-(chloromethyl)-4-fluorobenzene (826 μL, 6.90 mmol), and sodium carbonate (974 mg, 9.19 mmol) in DMF (20 mL) was stirred at 70 °C for 4 h. The solution was diluted with water and extracted with EtOAc (100 mL × 3). The organic layers were combined and washed with brine, dried over sodium sulfate, filtered, and concentrated. The residue was purified by flash silica chromatography (0–2.5% MeOH in CH₂Cl₂) to provide **31** as a light-yellow solid (1.46 g, 77.4%), mp 187–188 °C. ¹H NMR (300 MHz, CD₃OD): δ 7.35 (d, *J* = 7.5 Hz, 1H), 7.17–7.08 (m, 2H), 7.04 (t, *J* = 7.8 Hz, 3H), 7.00–6.95 (m, 2H), 5.27 (s, 2H), 4.50–4.43 (m, 1H), 3.84–3.60 (m, 1H), 3.47–3.39 (m, 2H), 3.37–3.33 (m, 1H), 2.24 (dt, *J* = 14.6, 6.7 Hz, 1H), 2.11–2.02 (m, 1H), 1.45 (s, 9H). ESI-MS *m/z*: [M + H]⁺ 411.3.

1-(4-Fluorobenzyl)-N-(pyrrolidin-3-yl)-1H-benzo[d]imidazole-2-amine (32). A solution of 31 (1.44 g, 3.51 mmol) in CH₂Cl₂ (10 mL) was treated with TFA (2.61 mL, 35.1 mmol). The mixture was stirred overnight at rt. The resulting solution was diluted with water, basified with sodium bicarbonate, and extracted with CH₂Cl₂ (60 mL × 3). The organic layers were combined and washed with brine, dried over sodium sulfate, filtered, and concentrated. The residue was purified by flash silica chromatography (0–8% MeOH in CH₂Cl₂) to give 32 as a yellow solid (875 mg, 80.4%), mp 202 °C. ¹H NMR (400 MHz, DMSO-*d*₆): δ 9.44 (s, 1H), 7.47 (s, 1H), 7.32–7.25 (m, 3H), 7.15 (d, *J* = 8.9 Hz, 2H), 7.13–7.11 (m, 1H), 6.98 (td, *J* = 7.6, 1.2 Hz, 1H), 6.89 (td, *J* = 7.6, 1.2 Hz, 1H), 5.36 (s, 2H), 4.67–4.45 (m, 1H), 3.48 (dd, *J* = 11.9, 6.5 Hz, 1H), 3.40 (dt, *J* = 11.5, 7.6 Hz, 1H), 3.34–3.23 (m, 2H), 2.32–2.20 (m, 1H), 2.16–2.03 (m, 1H). ESI-MS *m/z*: [M + H]⁺ 311.2.

4-Methoxyphenethyl 4-Methylbenzenesulfonate (33). A mixture of phenethyl alcohol (5.00 g, 32.9 mmol), tosyl chloride (9.39 g, 49.3 mmol), and triethylamine (13.7 mL, 98.6 mmol) in CH₂Cl₂ (80 mL) was stirred overnight at rt. The resulting solution was concentrated and purified by flash silica chromatography (0–8% EtOAc in PE) to provide 33 as a white solid (9.98 g, 99.2%), mp 58 °C. ¹H NMR (300 MHz, DMSO-*d*₆): δ 7.67 (d, *J* = 8.3 Hz, 2H), 7.42 (d, *J* = 8.0 Hz, 2H), 7.05 (d, *J* = 8.6 Hz, 2H), 6.81 (d, *J* = 8.6 Hz, 2H), 4.17 (t, *J* = 6.6 Hz, 2H), 3.72 (s, 3H), 2.80 (t, *J* = 6.5 Hz, 2H), 2.41 (s, 3H). ESI-MS *m/z*: [M + Na]⁺ 329.1.

1-(4-Fluorobenzyl)-N-(1-(4-methoxyphenethyl)pyrrolidin-3-yl)-1H-benzo[d]imidazole-2-amine (21, DC-PRC2in-01). A mixture of 32 (30 mg, 96.7 μmol), 33 (44 mg, 145.0 μmol), sodium carbonate (31 mg, 290 μmol), and potassium iodide (3 mg, 19.3 μmol) in DMF (2 mL) was stirred at 80 °C for 1 h. The solution was diluted with water and extracted with EtOAc (20 mL × 3). The organic layers were combined and washed with brine, dried over sodium sulfate, filtered, and concentrated. The residue was purified by flash silica chromatography (0–3% MeOH in CH₂Cl₂) to afford a light-yellow solid (31 mg, 72.1%), mp 124–125 °C. ¹H NMR (400 MHz, CDCl₃): δ 7.44 (d, *J* = 7.8 Hz, 1H), 7.15–7.06 (m, 5H), 7.02 (d, *J* = 3.7 Hz, 2H), 6.98 (t, *J* = 8.6 Hz, 2H), 6.81 (d, *J* = 8.5 Hz, 2H), 5.09 (s, 2H), 4.75–4.53 (m, 1H), 3.76 (s, 3H), 3.18–3.05 (m, 1H), 3.01 (d, *J* = 10.1 Hz, 1H), 2.84–2.71 (m, 4H), 2.66 (dd, *J* = 10.1, 6.2 Hz, 1H), 2.46–2.37 (m, 1H), 2.35–2.29 (m, 1H), 1.85–1.63 (m, 1H). ¹³C NMR (151 MHz, CDCl₃): δ 162.4 (d, *J* = 246.7 Hz), 158.2, 153.6, 142.0, 134.6, 131.5 (2C), 129.6 (2C), 128.6, 128.5, 121.7, 120.1, 116.5, 116.1, 116.0, 114.0 (2C), 107.6, 61.1, 57.5, 55.4, 52.9, 52.4, 45.1, 34.0, 32.5. HRMS (ESI/QTOF) *m/z*: [M + H]⁺ calcd for C₂₇H₃₀FN₄O: 445.2398; found, 445.2409. HPLC purity: 98.5%.

Protein Expression and Purification. For the crystallization study of EED with ligands, the gene of human EED (amino acids 40–441) was subcloned into a modified pET28GST-LIC vector, and transformed in *Escherichia coli* BL21 (DE3) Codon plus RIL. The bacteria with recombinant plasmid were cultured at 37 °C to OD₆₀₀ at 1.5, and induced by 0.2 mM IPTG to protein overexpression at 16 °C. The N-terminal GST-tagged EED protein was purified by affinity chromatography on glutathione-sepharose (GE Healthcare). After cleavage using thrombin (Sigma-Aldrich) on the column at 25 °C overnight, the flow-through was collected and purified further by size exclusion chromatography (Superdex 200, GE Healthcare). The purified EED proteins was concentrated to 10–15 mg/mL and stored at –80 °C in a buffer containing 20 mM Tris–HCl pH 7.5, 200 mM NaCl, and 1 mM DTT for further use in crystallization. For the FP, NMR, and SPR binding assays, the recombinant human EED (residues 81–441) with N-terminal 6× His-SUMO tag was overexpressed and purified as previously reported.^{47,51}

Crystallization and Structure Determination. Purified EED protein (aa 40–441) was mixed with 2-fold molar excess astemizole and crystallized by using the sitting drop vapor diffusion method at 18 °C. The complex of EED (aa 40–441) and astemizole was crystallized in a buffer containing 3.5 M sodium formate, 0.1 M Tris–HCl, pH 8.5. After optimized by detergents, the small needle crystals grew into diffracting crystals for structural determination. Before freezing in

liquid nitrogen, the crystals were immersed into a mixture consisting of reservoir solution plus 10% glycerol (v/v).

Data Collection and Structure Determination. X-ray diffraction data for EED were collected at 100 K at beamline 19D of Advanced Photon Source (APS), Argonne National Laboratory, and reduced with XDS⁶¹ and AIMLESS.⁶² The structure was solved by molecular replacement with coordinates from PDB entry 3JZN.⁶³ The model was iteratively refined with REFMAC⁶⁴ and PHENIX,⁶⁵ and rebuilt with COOT.⁶⁶ Model geometry was evaluated with MOLPROBITY.⁶⁷

Fluorescence Polarization Competition Assay. A previously described method was used to determine the inhibition activity of EZH2–EED interaction inhibitors.^{47,51} Briefly, the compounds were 2-fold serial diluted in DMSO, and added into a mixture of 0.6 μM EED protein and 20 nM FITC-labeled EZH2 (aa 40–63) peptide tracer in 40 μL of FP buffer (25 mM PIPES pH 6.2, 150 mM NaCl, 0.1 mg/mL BSA, and 0.01% NP40). The final concentrations of compounds range from 0.49 to 500 μM. After 2 h incubation at room temperature (25 °C), the FP values were recorded on a EnVision multimode plate reader (PerkinElmer). The IC₅₀ values were calculated by GraphPad Prism 6 using the mode of 4-parameter logistic nonlinear regression.

NMR-Based Binding Assay. The procedure of ligand T1ρ and STD NMR data acquisition was as previously described.⁵¹ Briefly, 200 μM compound in the absence or in the presence of 5 μM EED (aa 81–441) protein without or with 20, 50, or 100 μM EZH2 peptide (residues 39–68) were prepared in phosphate buffer (20 mM NaPO₄, 100 mM NaCl, pH 7.4, 10% DMSO) and measured at 25 °C on a 600 MHz Bruker Avance III NMR equipment (Bruker BioSpin, Germany).

Surface Plasmon Resonance (SPR)-Based Binding Assay. To determine the binding affinities of compounds to EED protein, the surface plasmon resonance platform Biacore T200 (GE Healthcare) was applied. Freshly purified EED (aa 81–441) proteins were immobilized on a CM5 sensor chip with a 10,000 response unit (RU). First, the compound stock 10 mM in DMSO was 100-fold diluted in HBS buffer (20 mM HEPES, pH 7.5, 150 mM NaCl, 0.1% Tween-20), and then 2-fold serial diluted in HBS buffer containing 1% DMSO. The final concentrations of compound range from 0.78 to 100 μM. The binding and dissociation times of compound injection were set as 120 and 240 s, respectively. The DDK_d values of the compounds were calculated by Biacore T200 evaluation software (GE Healthcare) using the kinetic modeling approach.

Molecular Docking. The crystal structure of EED protein (aa 40–441) complexed with astemizole (PDB ID: 7KXT) was used to construct a molecular docking model. Glide program (Schrödinger, LLC, New York, NY, 2015) 5.5^{68,69} was employed to perform molecular docking simulations. After the coordinates of protein were prepared by the Protein Preparation Wizard Workflow with default settings, the docking grid was generated by defining residues located within 20 Å around astemizole with the Receptor Grid Generation panel. Finally, the prepared compound (DC-PRC2in-01) that had been prepared with LigPrep (version 2.3, Schrödinger, LLC, New York, NY) was docked to the aforementioned docking grid with Extra precision (XP) mode. The top 1 docking pose ranked by the XP G-score was selected for binding mode analysis.

Cell Culture. All cell lines were maintained in a humidified incubator at 37 °C containing 5% CO₂ and 95% air. Diffused large B-cell lymphoma (DLBCL) cell lines (Pfeiffer, SU-DHL-4, Karspa-422, and DB) were obtained from the American Type Culture Collection (ATCC) and cultured in RPMI-1640 complete medium (containing 10% FBS and 1× Pen/Strep).

Cell Viability Assay. To determine the growth inhibition IC₅₀ of compounds, DLBCL cell lines were treated with a 9-point 2-fold dilution series of compounds or 0.1% DMSO. The seeding densities of each cell line in a 96-well format were empirically adjusted to 1–2 × 10⁴ cells per well (in duplicate). After 3 days of culture, the CellTiter-Glo (CTG) reagents (Promega) were used to measure the cell viability and data were processed using GraphPad Prism 6.

Western Blotting Analysis. To monitor the effects of compounds on PRC2 core components, H3K27me3 levels, and other histone H3 lysine trimethylation marks, Pfeiffer cells were cultured in the presence of different concentrations of compounds or 0.1% DMSO for 3 days. The cells were lysed in RIPA lysis buffer, and 30 μ g total proteins in cell lysates were separated on 4–12% SDS-PAGE and transferred onto nitrocellulose (NC) membranes. After blocking in 5% nonfat milk, the blotted NC membranes were incubated with primary antibodies stated in the figures at 4 °C overnight, followed by the incubation of HRP-linked secondary antibodies. The detection of blots was performed on an Amersham Imager 600 imaging system (GE Healthcare) using Pierce Western Blotting ECL Substrate (Thermo Scientific).

Cell Cycle Assay. PI/RNase Staining Buffer (BD Pharmingen) was used for the cell cycle assay. Pfeiffer and SU-DHL-4 cells were treated for 2 and 3 days, respectively, with 0.1% DMSO or different concentrations of compounds. Cells were washed with PBS and stained with PI according to the manufacturer's protocol. The samples were detected on a ZES Cell Analyzer (Bio-Rad), and data analysis was performed with software ModFit LT.

■ ASSOCIATED CONTENT

SI Supporting Information

The Supporting Information is available free of charge at <https://pubs.acs.org/doi/10.1021/acs.jmedchem.0c02261>.

Spectra of DC-PRC2in-01; synthetic procedures of compounds except DC-PRC2in-01; binding model of PRC2 inhibitors against the PRC2 core complex; STD NMR spectra of DC-PRC2in-01 with and without EED; molecular docking model of DC-PRC2in-01 with EED; and PDB coordinates of hydrogen-suppressed atomic model for DC-PRC2in-01 with EED (PDF)
Molecular formula strings (CSV) (CSV)

Accession Codes

Coordinates of the complexed structure of EED and astemizole have been deposited into Protein Data Bank with an ID of 7KXT. The atomic coordinates will be released upon the publication of this article.

■ AUTHOR INFORMATION

Corresponding Authors

Sergio Valente – Department of Drug Chemistry and Technologies, Sapienza University of Rome, Rome 00185, Italy; orcid.org/0000-0002-2241-607X;
Email: sergio.valente@uniroma1.it

Jinrong Min – Structural Genomics Consortium and Department of Physiology, University of Toronto, Toronto MSG1L7, Ontario, Canada; Hubei Key Laboratory of Genetic Regulation and Integrative Biology, School of Life Sciences, Central China Normal University, Wuhan 430079, China; Email: jr.min@utoronto.ca

Wenhu Duan – Department of Medicinal Chemistry, Shanghai Institute of Materia Medica, Chinese Academy of Sciences, Shanghai 201203, China; University of Chinese Academy of Sciences, Beijing 100049, China; orcid.org/0000-0002-5084-6026; Email: whduan@simm.ac.cn

Cheng Luo – School of Chinese Materia Medica, Nanjing University of Chinese Medicine, Nanjing 210023, Jiangsu, China; Drug Discovery and Design Center, the Center for Chemical Biology, State Key Laboratory of Drug Research, Shanghai Institute of Materia Medica, Chinese Academy of Sciences, Shanghai 210203, China; University of Chinese Academy of Sciences, Beijing 100049, China; School of Pharmacy, Key Laboratory of Molecular Pharmacology and

Drug Evaluation (Yantai University), Ministry of Education; Collaborative Innovation Center of Advanced Drug Delivery System and Biotech Drugs in Universities of Shandong, Yantai University, Yantai 264005, China; School of Pharmaceutical Science and Technology, Hangzhou Institute for Advanced Study, University of Chinese Academy of Sciences, Hangzhou 310024, China; orcid.org/0000-0003-3864-8382; Email: cluo@simm.ac.cn

Authors

Daohai Du – School of Chinese Materia Medica, Nanjing University of Chinese Medicine, Nanjing 210023, Jiangsu, China; Drug Discovery and Design Center, the Center for Chemical Biology, State Key Laboratory of Drug Research, Shanghai Institute of Materia Medica, Chinese Academy of Sciences, Shanghai 210203, China

Dandan Xu – Department of Medicinal Chemistry, Shanghai Institute of Materia Medica, Chinese Academy of Sciences, Shanghai 201203, China; University of Chinese Academy of Sciences, Beijing 100049, China

Licheng Zhu – Structural Genomics Consortium and Department of Physiology, University of Toronto, Toronto MSG1L7, Ontario, Canada; Hubei Key Laboratory of Genetic Regulation and Integrative Biology, School of Life Sciences, Central China Normal University, Wuhan 430079, China; School of Life Sciences, Jinggangshan University, Ji'an 343009, Jiangxi, China

Giulia Stazi – Department of Drug Chemistry and Technologies, Sapienza University of Rome, Rome 00185, Italy

Clemens Zwergel – Department of Drug Chemistry and Technologies, Sapienza University of Rome, Rome 00185, Italy; orcid.org/0000-0002-3097-0003

Yanli Liu – Structural Genomics Consortium and Department of Physiology, University of Toronto, Toronto MSG1L7, Ontario, Canada; Hubei Key Laboratory of Genetic Regulation and Integrative Biology, School of Life Sciences, Central China Normal University, Wuhan 430079, China; College of Pharmaceutical Sciences, Soochow University, Suzhou 215123, Jiangsu, China

Zhongyuan Luo – School of Chinese Materia Medica, Nanjing University of Chinese Medicine, Nanjing 210023, Jiangsu, China; Drug Discovery and Design Center, the Center for Chemical Biology, State Key Laboratory of Drug Research, Shanghai Institute of Materia Medica, Chinese Academy of Sciences, Shanghai 210203, China

Yuanqing Li – Drug Discovery and Design Center, the Center for Chemical Biology, State Key Laboratory of Drug Research, Shanghai Institute of Materia Medica, Chinese Academy of Sciences, Shanghai 210203, China; University of Chinese Academy of Sciences, Beijing 100049, China

Yuanyuan Zhang – Drug Discovery and Design Center, the Center for Chemical Biology, State Key Laboratory of Drug Research, Shanghai Institute of Materia Medica, Chinese Academy of Sciences, Shanghai 210203, China; orcid.org/0000-0002-4382-024X

Kongkai Zhu – School of Biological Science and Technology, University of Jinan, Jinan 250022, China

Yiluan Ding – Shanghai Institute of Materia Medica, Chinese Academy of Sciences, Shanghai 201203, China

Jingqiu Liu – Drug Discovery and Design Center, the Center for Chemical Biology, State Key Laboratory of Drug

Research, Shanghai Institute of Materia Medica, Chinese Academy of Sciences, Shanghai 210203, China

Shijie Fan – Drug Discovery and Design Center, the Center for Chemical Biology, State Key Laboratory of Drug Research, Shanghai Institute of Materia Medica, Chinese Academy of Sciences, Shanghai 210203, China

Kaiyan Zhao – Department of Medicinal Chemistry, Shanghai Institute of Materia Medica, Chinese Academy of Sciences, Shanghai 210203, China; University of Chinese Academy of Sciences, Beijing 100049, China

Naixia Zhang – Shanghai Institute of Materia Medica, Chinese Academy of Sciences, Shanghai 210203, China; orcid.org/0000-0003-4824-5819

Xiangqian Kong – Guangdong Provincial Key Laboratory of Biocomputing, Guangzhou Institutes of Biomedicine and Health, Chinese Academy of Sciences, Guangzhou 510530, China

Hualiang Jiang – Drug Discovery and Design Center, the Center for Chemical Biology, State Key Laboratory of Drug Research, Shanghai Institute of Materia Medica, Chinese Academy of Sciences, Shanghai 210203, China

Kaixian Chen – Drug Discovery and Design Center, the Center for Chemical Biology, State Key Laboratory of Drug Research, Shanghai Institute of Materia Medica, Chinese Academy of Sciences, Shanghai 210203, China

Kehao Zhao – School of Pharmacy, Key Laboratory of Molecular Pharmacology and Drug Evaluation (Yantai University), Ministry of Education; Collaborative Innovation Center of Advanced Drug Delivery System and Biotech Drugs in Universities of Shandong, Yantai University, Yantai 264005, China

Complete contact information is available at:

<https://pubs.acs.org/10.1021/acs.jmedchem.0c02261>

Author Contributions

[†]D.D., D.X. and L.Z. contributed equally. All authors have given approval to the final version of the manuscript.

Notes

The authors declare no competing financial interest.

ACKNOWLEDGMENTS

We thank Dr. Aiping Dong for assistance in structure determination. We are grateful to National Center for Protein Science Shanghai (Protein Expression and Purification system) for their instrument support and technical assistance. We also gratefully acknowledge the financial support from the National Natural Science Foundation of China (81821005, 91853205, and 81625022, to C.L.), K.C. Wong Education to C.L., the Science and Technology Commission of Shanghai Municipality (19XD1404700 and 18431907100 to C.L.), the Department of Science and Technology of Fujian Province (2019T3029 to C.L.), and National Science & Technology Major Project “Key New Drug Creation and Manufacturing Program” (2018ZX09711002 to C.L.). The Structural Genomics Consortium is a registered charity (no: 1097737) that receives funds from AbbVie, Bayer AG, Boehringer Ingelheim, Genentech, and Genome Canada through Ontario Genomics Institute [OGI-196], the EU and EFPIA through the Innovative Medicines Initiative 2 Joint Undertaking [EUBOPEN grant 875510], and Janssen, Merck KGaA (aka EMD in Canada and US), Pfizer, Takeda, and the Wellcome

Trust [106169/ZZ14/Z]. We are also grateful to Ateneo 2020 Sapienza Project (RG120172B8E53D03).

ABBREVIATIONS

PRC2, polycomb repressive complex 2; EZH2, enhancer of zeste homologue 2; EED, embryonic ectoderm development; SUZ12, suppressor of zeste 12 homologue; H3K27, histone H3 lysine 27; PPI, protein–protein interaction; EWG, electron-withdrawing group; SAM, S-adenosylmethionine; FP, fluorescence polarization; SPR, surface plasmon resonance

REFERENCES

- (1) Simon, J. A.; Kingston, R. E. Mechanisms of Polycomb gene silencing: knowns and unknowns. *Nat. Rev. Mol. Cell Biol.* **2009**, *10*, 697–708.
- (2) Margueron, R.; Reinberg, D. The Polycomb complex PRC2 and its mark in life. *Nature* **2011**, *469*, 343–349.
- (3) Kouznetsova, V. L.; Tchekhanov, A.; Li, X.; Yan, X.; Tsigelny, I. F. Polycomb repressive 2 complex-molecular mechanisms of function. *Protein Sci.* **2019**, *28*, 1387–1399.
- (4) Yu, J.-R.; Lee, C.-H.; Oksuz, O.; Stafford, J. M.; Reinberg, D. PRC2 is high maintenance. *Genes Dev.* **2019**, *33*, 903–935.
- (5) Comet, I.; Riising, E. M.; Leblanc, B.; Helin, K. Maintaining cell identity: PRC2-mediated regulation of transcription and cancer. *Nat. Rev. Cancer* **2016**, *16*, 803–810.
- (6) He, A.; Ma, Q.; Cao, J.; von Gise, A.; Zhou, P.; Xie, H.; Zhang, B.; Hsing, M.; Christodoulou, D. C.; Cahan, P.; Daley, G. Q.; Kong, S. W.; Orkin, S. H.; Seidman, C. E.; Seidman, J. G.; Pu, W. T. Polycomb repressive complex 2 regulates normal development of the mouse heart. *Circ. Res.* **2012**, *110*, 406–415.
- (7) Czermin, B.; Melfi, R.; McCabe, D.; Seitz, V.; Imhof, A.; Pirrotta, V. Drosophila enhancer of Zeste/ESC complexes have a histone H3 methyltransferase activity that marks chromosomal Polycomb sites. *Cell* **2002**, *111*, 185–196.
- (8) Cao, R.; Zhang, Y. SUZ12 is required for both the histone methyltransferase activity and the silencing function of the EED-EZH2 complex. *Mol. Cell* **2004**, *15*, 57–67.
- (9) Chamberlain, S. J.; Yee, D.; Magnuson, T. Polycomb repressive complex 2 is dispensable for maintenance of embryonic stem cell pluripotency. *Stem Cell* **2008**, *26*, 1496–1505.
- (10) Gao, Z.; Zhang, J.; Bonasio, R.; Strino, F.; Sawai, A.; Parisi, F.; Kluger, Y.; Reinberg, D. PCGF homologs, CBX proteins, and RYBP define functionally distinct PRC1 family complexes. *Mol. Cell* **2012**, *45*, 344–356.
- (11) Hauri, S.; Comoglio, F.; Seimiya, M.; Gerstung, M.; Glatter, T.; Hansen, K.; Aebersold, R.; Paro, R.; Gstaiger, M.; Beisel, C. A High-Density Map for Navigating the Human Polycomb Complexome. *Cell Rep.* **2016**, *17*, 583–595.
- (12) Brooun, A.; Gajiwala, K. S.; Deng, Y. L.; Liu, W.; Bolanos, B.; Bingham, P.; He, Y. A.; Diehl, W.; Grable, N.; Kung, P. P.; Sutton, S.; Maegley, K. A.; Yu, X.; Stewart, A. E. Polycomb repressive complex 2 structure with inhibitor reveals a mechanism of activation and drug resistance. *Nat. Commun.* **2016**, *7*, 11384.
- (13) Jiao, L.; Liu, X. Structural basis of histone H3K27 trimethylation by an active Polycomb repressive complex 2. *Science* **2015**, *350*, aac4383.
- (14) Margueron, R.; Justin, N.; Ohno, K.; Sharpe, M. L.; Son, J., 3rd; Drury, W. J., 3rd; Voigt, P.; Martin, S. R.; Taylor, W. R.; De Marco, V.; Pirrotta, V.; Reinberg, D.; Gamblin, S. J. Role of the Polycomb protein EED in the propagation of repressive histone marks. *Nature* **2009**, *461*, 762–767.
- (15) Chase, A.; Cross, N. C. P. Aberrations of EZH2 in Cancer: Figure 1. *Clin. Cancer Res.* **2011**, *17*, 2613–2618.
- (16) Chang, C.-J.; Hung, M.-C. The role of EZH2 in tumour progression. *Br. J. Cancer* **2012**, *106*, 243–247.
- (17) Duan, R.; Du, W.; Guo, W. EZH2 a novel target for cancer treatment. *J. Hematol. Oncol.* **2020**, *13*, 104.

- (18) Varambally, S.; Dhanasekaran, S. M.; Zhou, M.; Barrette, T. R.; Kumar-Sinha, C.; Sanda, M. G.; Ghosh, D.; Pienta, K. J.; Sewalt, R. G. A. B.; Otte, A. P.; Rubin, M. A.; Chinnaiyan, A. M. The Polycomb group protein EZH2 is involved in progression of prostate cancer. *Nature* **2002**, *419*, 624–629.
- (19) Kleer, C. G.; Cao, Q.; Varambally, S.; Shen, R.; Ota, I.; Tomlins, S. A.; Ghosh, D.; Sewalt, R. G. A. B.; Otte, A. P.; Hayes, D. F.; Sabel, M. S.; Livant, D.; Weiss, S. J.; Rubin, M. A.; Chinnaiyan, A. M. EZH2 is a marker of aggressive breast cancer and promotes neoplastic transformation of breast epithelial cells. *Proc. Natl. Acad. Sci. U.S.A.* **2003**, *100*, 11606–11611.
- (20) Ohuchi, M.; Sakamoto, Y.; Tokunaga, R.; Kiyozumi, Y.; Nakamura, K.; Izumi, D.; Kosumi, K.; Harada, K.; Kurashige, J.; Iwatsuki, M.; Baba, Y.; Miyamoto, Y.; Yoshida, N.; Shono, T.; Naoe, H.; Sasaki, Y.; Baba, H. Increased EZH2 expression during the adenoma-carcinoma sequence in colorectal cancer. *Oncol. Lett.* **2018**, *16*, 5275–5281.
- (21) Li, H.; Cai, Q.; Godwin, A. K.; Zhang, R. Enhancer of zeste homolog 2 promotes the proliferation and invasion of epithelial ovarian cancer cells. *Mol. Cancer Res.* **2010**, *8*, 1610–1618.
- (22) Kemp, C. D.; Rao, M.; Xi, S.; Inchauste, S.; Mani, H.; Fetsch, P.; Filie, A.; Zhang, M.; Hong, J. A.; Walker, R. L.; Zhu, Y. J.; Ripley, R. T.; Mathur, A.; Liu, F.; Yang, M.; Meltzer, P. A.; Marquez, V. E.; De Rienzo, A.; Bueno, R.; Schrupp, D. S. Polycomb repressor complex-2 is a novel target for mesothelioma therapy. *Clin. Cancer Res.* **2012**, *18*, 77–90.
- (23) Wagener, N.; Macher-Goeppinger, S.; Pritsch, M.; Hüsing, J.; Hoppe-Seyler, K.; Schirmacher, P.; Pfitzenmaier, J.; Haferkamp, A.; Hoppe-Seyler, F.; Hohenfellner, M. Enhancer of zeste homolog 2 (EZH2) expression is an independent prognostic factor in renal cell carcinoma. *BMC Canc.* **2010**, *10*, 524.
- (24) Morin, R. D.; Johnson, N. A.; Severson, T. M.; Mungall, A. J.; An, J.; Goya, R.; Paul, J. E.; Boyle, M.; Woolcock, B. W.; Kuchenbauer, F.; Yap, D.; Humphries, R. K.; Griffith, O. L.; Shah, S.; Zhu, H.; Kimbara, M.; Shashkin, P.; Charlot, J. F.; Tcherpakov, M.; Corbett, R.; Tam, A.; Varhol, R.; Smailus, D.; Moksa, M.; Zhao, Y.; Delaney, A.; Qian, H.; Birol, I.; Schein, J.; Moore, R.; Holt, R.; Horsman, D. E.; Connors, J. M.; Jones, S.; Aparicio, S.; Hirst, M.; Gascogne, R. D.; Marra, M. A. Somatic mutations altering EZH2 (Tyr641) in follicular and diffuse large B-cell lymphomas of germinal-center origin. *Nat. Genet.* **2010**, *42*, 181–185.
- (25) Lohr, J. G.; Stojanov, P.; Lawrence, M. S.; Auclair, D.; Chapuy, B.; Sougnez, C.; Cruz-Gordillo, P.; Knoechel, B.; Asmann, Y. W.; Slager, S. L.; Novak, A. J.; Dogan, A.; Ansell, S. M.; Link, B. K.; Zou, L.; Gould, J.; Saksena, G.; Stransky, N.; Rangel-Escareño, C.; Fernandez-Lopez, J. C.; Hidalgo-Miranda, A.; Melendez-Zajgla, J.; Hernández-Lemus, E.; Schwarz-Cruz y Celis, A.; Imaz-Rosshandler, I.; Ojesina, A. I.; Jung, J.; Peadarallu, C. S.; Lander, E. S.; Habermann, T. M.; Cerhan, J. R.; Shipp, M. A.; Getz, G.; Golub, T. R. Discovery and prioritization of somatic mutations in diffuse large B-cell lymphoma (DLBCL) by whole-exome sequencing. *Proc. Natl. Acad. Sci. U.S.A.* **2012**, *109*, 3879–3884.
- (26) Bödör, C.; Grossmann, V.; Popov, N.; Okosun, J.; O’Riain, C.; Tan, K.; Marzec, J.; Araf, S.; Wang, J.; Lee, A. M.; Clear, A.; Montoto, S.; Matthews, J.; Iqbal, S.; Rajnai, H.; Rosenwald, A.; Ott, G.; Campo, E.; Rimsza, L. M.; Smeland, E. B.; Chan, W. C.; Brazier, R. M.; Staudt, L. M.; Wright, G.; Lister, T. A.; Elemento, O.; Hills, R.; Gribben, J. G.; Chelala, C.; Matolcsy, A.; Kohlmann, A.; Haferlach, T.; Gascogne, R. D.; Fitzgibbon, J. EZH2 mutations are frequent and represent an early event in follicular lymphoma. *Blood* **2013**, *122*, 3165–3168.
- (27) Kim, K. H.; Roberts, C. W. M. Targeting EZH2 in cancer. *Nat. Med.* **2016**, *22*, 128–134.
- (28) Knutson, S. K.; Wigle, T. J.; Warholc, N. M.; Sneeringer, C. J.; Allain, C. J.; Klaus, C. R.; Sacks, J. D.; Raimondi, A.; Majer, C. R.; Song, J.; Scott, M. P.; Jin, L.; Smith, J. J.; Olhava, E. J.; Chesworth, R.; Moyer, M. P.; Richon, V. M.; Copeland, R. A.; Keilhack, H.; Pollock, R. M.; Kuntz, K. W. A selective inhibitor of EZH2 blocks H3K27 methylation and kills mutant lymphoma cells. *Nat. Chem. Biol.* **2012**, *8*, 890–896.
- (29) Qi, W.; Chan, H.; Teng, L.; Li, L.; Chuai, S.; Zhang, R.; Zeng, J.; Li, M.; Fan, H.; Lin, Y.; Gu, J.; Ardayfio, O.; Zhang, J.-H.; Yan, X.; Fang, J.; Mi, Y.; Zhang, M.; Zhou, T.; Feng, G.; Chen, Z.; Li, G.; Yang, T.; Zhao, K.; Liu, X.; Yu, Z.; Lu, C. X.; Atadja, P.; Li, E. Selective inhibition of Ezh2 by a small molecule inhibitor blocks tumor cells proliferation. *Proc. Natl. Acad. Sci. U.S.A.* **2012**, *109*, 21360–21365.
- (30) Konze, K. D.; Ma, A.; Li, F.; Barsyte-Lovejoy, D.; Parton, T.; Macnevin, C. J.; Liu, F.; Gao, C.; Huang, X.-P.; Kuznetsova, E.; Rougie, M.; Jiang, A.; Pattenden, S. G.; Norris, J. L.; James, L. I.; Roth, B. L.; Brown, P. J.; Frye, S. V.; Arrowsmith, C. H.; Hahn, K. M.; Wang, G. G.; Vedadi, M.; Jin, J. An orally bioavailable chemical probe of the lysine methyltransferases EZH2 and EZH1. *ACS Chem. Biol.* **2013**, *8*, 1324–1334.
- (31) Yang, X.; Li, F.; Konze, K. D.; Meslamani, J.; Ma, A.; Brown, P. J.; Zhou, M.-M.; Arrowsmith, C. H.; Kaniskan, H. Ü.; Vedadi, M.; Jin, J. Structure-activity relationship studies for enhancer of zeste homologue 2 (EZH2) and enhancer of zeste homologue 1 (EZH1) inhibitors. *J. Med. Chem.* **2016**, *59*, 7617–7633.
- (32) Kung, P.-P.; Bingham, P.; Brooun, A.; Collins, M.; Deng, Y.-L.; Dinh, D.; Fan, C.; Gajiwala, K. S.; Grantner, R.; Gukasyan, H. J.; Hu, W.; Huang, B.; Kania, R.; Kephart, S. E.; Krivacic, C.; Kumpf, R. A.; Khamphavong, P.; Kraus, M.; Liu, W.; Maegley, K. A.; Nguyen, L.; Ren, S.; Richter, D.; Rollins, R. A.; Sach, N.; Sharma, S.; Sherrill, J.; Spangler, J.; Stewart, A. E.; Sutton, S.; Uryu, S.; Verhelle, D.; Wang, H.; Wang, S.; Wythes, M.; Xin, S.; Yamazaki, S.; Zhu, H.; Zhu, J.; Zehnder, L.; Edwards, M. Optimization of orally bioavailable enhancer of zeste homolog 2 (EZH2) inhibitors using ligand and property-based design strategies: identification of development candidate (R)-5,8-dichloro-7-(methoxy(oxetan-3-yl)methyl)-2-((4-methoxy-6-methyl-2-oxo-1,2-dihydropyridin-3-yl)methyl)-3,4-dihydroisoquinolin-1(2H)-one (PF-06821497). *J. Med. Chem.* **2018**, *61*, 650–665.
- (33) Fioravanti, R.; Stazi, G.; Zwergel, C.; Valente, S.; Mai, A. Six Years (2012–2018) of Researches on Catalytic EZH2 Inhibitors: The Boom of the 2-Pyridone Compounds. *Chem. Rec.* **2018**, *18*, 1818–1832.
- (34) McCabe, M. T.; Ott, H. M.; Ganji, G.; Korenchuk, S.; Thompson, C.; Van Aller, G. S.; Liu, Y.; Graves, A. P.; Iii, A. D. P., 3rd; Diaz, E.; LaFrance, L. V.; Mellinger, M.; Duquenne, C.; Tian, X.; Kruger, R. G.; McHugh, C. F.; Brandt, M.; Miller, W. H.; Dhanak, D.; Verma, S. K.; Tummino, P. J.; Creasy, C. L. EZH2 inhibition as a therapeutic strategy for lymphoma with EZH2-activating mutations. *Nature* **2012**, *492*, 108–112.
- (35) Vaswani, R. G.; Gehling, V. S.; Dakin, L. A.; Cook, A. S.; Nasveschuk, C. G.; Duplessis, M.; Iyer, P.; Balasubramanian, S.; Zhao, F.; Good, A. C.; Campbell, R.; Lee, C.; Cantone, N.; Cummings, R. T.; Normant, E.; Bellon, S. F.; Albrecht, B. K.; Harmange, J.-C.; Trojer, P.; Audia, J. E.; Zhang, Y.; Justin, N.; Chen, S.; Wilson, J. R.; Gambin, S. J. Identification of (R)-N-((4-methoxy-6-methyl-2-oxo-1,2-dihydropyridin-3-yl)methyl)-2-methyl-1-(1-(1-(2,2,2-trifluoroethyl)piperidin-4-yl)ethyl)-1H-indole-3-carboxamide (CPI-1205), a potent and selective inhibitor of histone methyltransferase EZH2, suitable for phase I clinical trials for B-cell lymphomas. *J. Med. Chem.* **2016**, *59*, 9928–9941.
- (36) Knutson, S. K.; Kawano, S.; Minoshima, Y.; Warholc, N. M.; Huang, K.-C.; Xiao, Y.; Kadowaki, T.; Uesugi, M.; Kuznetsov, G.; Kumar, N.; Wigle, T. J.; Klaus, C. R.; Allain, C. J.; Raimondi, A.; Waters, N. J.; Smith, J. J.; Porter-Scott, M.; Chesworth, R.; Moyer, M. P.; Copeland, R. A.; Richon, V. M.; Uenaka, T.; Pollock, R. M.; Kuntz, K. W.; Yokoi, A.; Keilhack, H. Selective inhibition of EZH2 by EPZ-6438 leads to potent antitumor activity in EZH2-mutant non-Hodgkin lymphoma. *Mol. Cancer Ther.* **2014**, *13*, 842–854.
- (37) Italiano, A.; Soria, J.-C.; Toulmonde, M.; Michot, J.-M.; Lucchesi, C.; Varga, A.; Coindre, J.-M.; Blakemore, S. J.; Clawson, A.; Suttle, B.; McDonald, A. A.; Woodruff, M.; Ribich, S.; Hedrick, E.; Keilhack, H.; Thomson, B.; Owa, T.; Copeland, R. A.; Ho, P. T. C.; Ribrag, V. Tazemetostat, an EZH2 inhibitor, in relapsed or refractory

B-cell non-Hodgkin lymphoma and advanced solid tumours: a first-in-human, open-label, phase 1 study. *Lancet Oncol.* **2018**, *19*, 649–659.

(38) Martin, M. C.; Zeng, G.; Yu, J.; Schiltz, G. E. Small molecule approaches for targeting the Polycomb repressive complex 2 (PRC2) in cancer. *J. Med. Chem.* **2020**, *63*, 15344.

(39) Hoy, S. M. Tazemetostat: first approval. *Drugs* **2020**, *80*, 513–521.

(40) Yang, C.-Y.; Wang, S. Allosteric inactivation of Polycomb repressive complex 2 (PRC2) by inhibiting its adapter protein: embryonic ectoderm development (EED). *J. Med. Chem.* **2017**, *60*, 2212–2214.

(41) Bisselier, M.; Wajapeyee, N. Mechanisms of resistance to EZH2 inhibitors in diffuse large B-cell lymphomas. *Blood* **2018**, *131*, 2125–2137.

(42) Qi, W.; Zhao, K.; Gu, J.; Huang, Y.; Wang, Y.; Zhang, H.; Zhang, M.; Zhang, J.; Yu, Z.; Li, L.; Teng, L.; Chuai, S.; Zhang, C.; Zhao, M.; Chan, H.; Chen, Z.; Fang, D.; Fei, Q.; Feng, L.; Feng, L.; Gao, Y.; Ge, H.; Ge, X.; Li, G.; Lingel, A.; Lin, Y.; Liu, Y.; Luo, F.; Shi, M.; Wang, L.; Wang, Z.; Yu, Y.; Zeng, J.; Zeng, C.; Zhang, L.; Zhang, Q.; Zhou, S.; Oyang, C.; Atadja, P.; Li, E. An allosteric PRC2 inhibitor targeting the H3K27me3 binding pocket of EED. *Nat. Chem. Biol.* **2017**, *13*, 381–388.

(43) Huang, Y.; Zhang, J.; Yu, Z.; Zhang, H.; Wang, Y.; Lingel, A.; Qi, W.; Gu, J.; Zhao, K.; Shultz, M. D.; Wang, L.; Fu, X.; Sun, Y.; Zhang, Q.; Jiang, X.; Zhang, J.; Zhang, C.; Li, L.; Zeng, J.; Feng, L.; Zhang, C.; Liu, Y.; Zhang, M.; Zhang, L.; Zhao, M.; Gao, Z.; Liu, X.; Fang, D.; Guo, H.; Mi, Y.; Gabriel, T.; Dillon, M. P.; Atadja, P.; Oyang, C. Discovery of first-in-class, potent, and orally bioavailable embryonic ectoderm development (EED) inhibitor with robust anticancer efficacy. *J. Med. Chem.* **2017**, *60*, 2215–2226.

(44) He, Y.; Selvaraju, S.; Curtin, M. L.; Jakob, C. G.; Zhu, H.; Comess, K. M.; Shaw, B.; The, J.; Lima-Fernandes, E.; Szweczyk, M. M.; Cheng, D.; Klinge, K. L.; Li, H.-Q.; Pliushchev, M.; Algire, M. A.; Maag, D.; Guo, J.; Dietrich, J.; Panchal, S. C.; Petros, A. M.; Sweis, R. F.; Torrent, M.; Bigelow, L. J.; Senisterra, G.; Li, F.; Kennedy, S.; Wu, Q.; Osterling, D. J.; Lindley, D. J.; Gao, W.; Galasinski, S.; Barsyte-Lovejoy, D.; Vedadi, M.; Buchanan, F. G.; Arrowsmith, C. H.; Chiang, G. G.; Sun, C.; Pappano, W. N. The EED protein-protein interaction inhibitor A-395 inactivates the PRC2 complex. *Nat. Chem. Biol.* **2017**, *13*, 389–395.

(45) Dong, H.; Liu, S.; Zhang, X.; Chen, S.; Kang, L.; Chen, Y.; Ma, S.; Fu, X.; Liu, Y.; Zhang, H.; Zou, B. An allosteric PRC2 inhibitor targeting EED suppresses tumor progression by modulating the immune response. *Cancer Res.* **2019**, *79*, 5587–5596.

(46) Rej, R. K.; Wang, C.; Lu, J.; Wang, M.; Petrunak, E.; Zawacki, K. P.; McEachern, D.; Fernandez-Salas, E.; Yang, C.-Y.; Wang, L.; Li, R.; Chinnaswamy, K.; Wen, B.; Sun, D.; Stuckey, J.; Zhou, Y.; Chen, J.; Tang, G.; Wang, S. EEDi-5285: an exceptionally potent, efficacious, and orally active small-molecule inhibitor of embryonic ectoderm development. *J. Med. Chem.* **2020**, *63*, 7252–7267.

(47) Zhu, M.-r.; Du, D.-h.; Hu, J.-c.; Li, L.-c.; Liu, J.-q.; Ding, H.; Kong, X.-q.; Jiang, H.-l.; Chen, K.-x.; Luo, C. Development of a high-throughput fluorescence polarization assay for the discovery of EZH2-EED interaction inhibitors. *Acta Pharmacol. Sin.* **2018**, *39*, 302–310.

(48) Zhu, K.; Du, D.; Yang, R.; Tao, H.; Zhang, H. Identification and assessments of novel and potent small-molecule inhibitors of EED-EZH2 interaction of polycomb repressive complex 2 by computational methods and biological evaluations. *Chem. Pharm. Bull.* **2020**, *68*, 58–63.

(49) Han, Z.; Xing, X.; Hu, M.; Zhang, Y.; Liu, P.; Chai, J. Structural basis of EZH2 recognition by EED. *Structure* **2007**, *15*, 1306–1315.

(50) Kim, W.; Bird, G. H.; Neff, T.; Guo, G.; Kerényi, M. A.; Walensky, L. D.; Orkin, S. H. Targeted disruption of the EZH2-EED complex inhibits EZH2-dependent cancer. *Nat. Chem. Biol.* **2013**, *9*, 643–650.

(51) Kong, X.; Chen, L.; Jiao, L.; Jiang, X.; Lian, F.; Lu, J.; Zhu, K.; Du, D.; Liu, J.; Ding, H.; Zhang, N.; Shen, J.; Zheng, M.; Chen, K.; Liu, X.; Jiang, H.; Luo, C. Astemizole arrests the proliferation of

cancer cells by disrupting the EZH2-EED interaction of Polycomb repressive complex 2. *J. Med. Chem.* **2014**, *57*, 9512–9521.

(52) Catalano, R.; Rocca, R.; Juli, G.; Costa, G.; Maruca, A.; Artese, A.; Caracciolo, D.; Tagliaferri, P.; Alcaro, S.; Tassone, P.; Amodio, N. A drug repurposing screening reveals a novel epigenetic activity of hydroxychloroquine. *Eur. J. Med. Chem.* **2019**, *183*, 111715.

(53) Smith, M. C.; Gestwicki, J. E. Features of protein-protein interactions that translate into potent inhibitors: topology, surface area and affinity. *Expert Rev. Mol. Med.* **2012**, *14*, No. e16.

(54) Montgomery, N. D.; Yee, D.; Chen, A.; Kalantry, S.; Chamberlain, S. J.; Otte, A. P.; Magnuson, T. The murine Polycomb group protein Eed is required for global histone H3 lysine-27 methylation. *Curr. Biol.* **2005**, *15*, 942–947.

(55) Montgomery, N. D.; Yee, D.; Montgomery, S. A.; Magnuson, T. Molecular and functional mapping of EED motifs required for PRC2-dependent histone methylation. *J. Mol. Biol.* **2007**, *374*, 1145–1157.

(56) Denisenko, O.; Shnyreva, M.; Suzuki, H.; Bomsztyk, K. Point mutations in the WD40 domain of Eed block its interaction with Ezh2. *Mol. Cell. Biol.* **1998**, *18*, 5634.

(57) Hsu, J. H.-R.; Rasmusson, T.; Robinson, J.; Pachl, F.; Read, J.; Kawatkar, S.; O' Donovan, D. H.; Bagal, S.; Code, E.; Rawlins, P.; Argyrou, A.; Tomlinson, R.; Gao, N.; Zhu, X.; Chiarparin, E.; Jacques, K.; Shen, M.; Woods, H.; Bednarski, E.; Wilson, D. M.; Drew, L.; Castaldi, M. P.; Fawell, S.; Bloecher, A. EED-Targeted PROTACs Degrade EED, EZH2, and SUZ12 in the PRC2 Complex. *Cell Chem. Biol.* **2020**, *27*, 41–46.

(58) Potjewyd, F.; Turner, A.-M. W.; Beri, J.; Rectenwald, J. M.; Norris-Drouin, J. L.; Cholensky, S. H.; Margolis, D. M.; Pearce, K. H.; Herring, L. E.; James, L. I. Degradation of Polycomb Repressive Complex 2 with an EED-Targeted Bivalent Chemical Degradator. *Cell Chem. Biol.* **2020**, *27*, 47–56.

(59) Janssens, F.; Torremans, J.; Janssen, M.; Stokbroekx, R. A.; Luyckx, M.; Janssen, P. A. J. New antihistaminic N-heterocyclic 4-piperidinamines. 2. Synthesis and antihistaminic activity of 1-[(4-fluorophenyl)methyl]-N-(4-piperidinyl)-1H-benzimidazol-2-amine. *J. Med. Chem.* **1985**, *28*, 1934–1943.

(60) Perkins, J. J.; Zartman, A. E.; Meissner, R. S. Synthesis of 2-(alkylamino)benzimidazoles. *Tetrahedron Lett.* **1999**, *40*, 1103–1106.

(61) Kabsch, W. Xds. *Acta Crystallogr. Sect. D Biol. Crystallogr.* **2010**, *66*, 125–132.

(62) Evans, P. R.; Murshudov, G. N. How good are my data and what is the resolution? *Acta Crystallogr. Sect. D Biol. Crystallogr.* **2013**, *69*, 1204–1214.

(63) Xu, C.; Bian, C.; Yang, W.; Galka, M.; Ouyang, H.; Chen, C.; Qiu, W.; Liu, H.; Jones, A. E.; MacKenzie, F.; Pan, P.; Li, S. S.-C.; Wang, H.; Min, J. Binding of different histone marks differentially regulates the activity and specificity of Polycomb repressive complex 2 (PRC2). *Proc. Natl. Acad. Sci. U.S.A.* **2010**, *107*, 19266–19271.

(64) Murshudov, G. N.; Skubák, P.; Lebedev, A. A.; Pannu, N. S.; Steiner, R. A.; Nicholls, R. A.; Winn, M. D.; Long, F.; Vagin, A. A. REFMAC5 for the refinement of macromolecular crystal structures. *Acta Crystallogr. Sect. D Biol. Crystallogr.* **2011**, *67*, 355–367.

(65) Liebschner, D.; Afonine, P. V.; Baker, M. L.; Bunkóczi, G.; Chen, V. B.; Croll, T. I.; Hintze, B.; Hung, L.-W.; Jain, S.; McCoy, A. J.; Moriarty, N. W.; Oeffner, R. D.; Poon, B. K.; Prisant, M. G.; Read, R. J.; Richardson, J. S.; Richardson, D. C.; Sammito, M. D.; Sobolev, O. V.; Stockwell, D. H.; Terwilliger, T. C.; Urzhumtsev, A. G.; Videau, L. L.; Williams, C. J.; Adams, P. D. Macromolecular structure determination using X-rays, neutrons and electrons: recent developments in Phenix. *Acta Crystallogr., Sect. D: Struct. Biol.* **2019**, *75*, 861–877.

(66) Emsley, P.; Lohkamp, B.; Scott, W. G.; Cowtan, K. Features and development of Coot. *Acta Crystallogr. Sect. D Biol. Crystallogr.* **2010**, *66*, 486–501.

(67) Chen, V. B.; Arendall, W. B.; Headd, J. J.; Keedy, D. A.; Immormino, R. M.; Kapral, G. J.; Murray, L. W.; Richardson, J. S.; Richardson, D. C. MolProbity: all-atom structure validation for

macromolecular crystallography. *Acta Crystallogr. Sect. D Biol. Crystallogr.* **2010**, *66*, 12–21.

(68) Friesner, R. A.; Banks, J. L.; Murphy, R. B.; Halgren, T. A.; Klicic, J. J.; Mainz, D. T.; Repasky, M. P.; Knoll, E. H.; Shelley, M.; Perry, J. K.; Shaw, D. E.; Francis, P.; Shenkin, P. S. Glide: A New Approach for Rapid, Accurate Docking and Scoring. 1. Method and Assessment of Docking Accuracy. *J. Med. Chem.* **2004**, *47*, 1739–1749.

(69) Halgren, T. A.; Murphy, R. B.; Friesner, R. A.; Beard, H. S.; Frye, L. L.; Pollard, W. T.; Banks, J. L. Glide: A New Approach for Rapid, Accurate Docking and Scoring. 2. Enrichment Factors in Database Screening. *J. Med. Chem.* **2004**, *47*, 1750–1759.